Available online at www.sciencedirect.com
ScienceDirect
Polymer 48 (2007) 3822–3835
polymer
www.elsevier.com/locate/polymer

Transient and steady-state deformations and breakup of dispersed-phase droplets of immiscible polymer blends in steady shear flow

Puritat Tanpaiboonkul [a], Wanchai Lerdwijitjarud [b], Anuvat Sirivat [a,*], Ronald G. Larson [c]

[a] *Conductive and Electroactive Polymers Research Unit, The Petroleum and Petrochemical College, Chulalongkorn University, Soi Chula 12, Phyathai Road, Bangkok 10330, Thailand*

[b] *Department of Materials Science and Engineering, Faculty of Engineering and Industrial Technology, Silpakorn University, Nakhon Pathom 73000, Thailand*

[c] *Department of Chemical Engineering, University of Michigan, Ann Arbor, MI 48109, USA*

Received 3 April 2006; received in revised form 19 March 2007; accepted 15 April 2007
Available online 19 April 2007

Abstract

Transient and steady-state deformations and breakup of viscoelastic polystyrene droplets dispersed in viscoelastic high-density polyethylene matrices were observed in a simple steady shear flow between two transparent parallel disks. By separately varying the elasticities of the individual blend components, the matrix shear viscosity, and the viscosity ratio, their effects on the transient deformation, steady-state droplet size, and the breakup sequence were determined. After the startup of a steady shear flow, the viscoelastic droplet initially exhibits oscillations of its length in the flow direction, but eventually stretches preferentially in the vorticity direction. We find that at fixed capillary number, the oscillation amplitude decreases with increasing droplet elasticity, while the oscillation period depends primarily on, and increases with, the viscosity ratio. At steady-state, the droplet length along the vorticity direction increases with increasing capillary number, viscosity ratio, and droplet elasticity. Remarkably, at a viscosity ratio of unity, the droplets remain in a nearly undeformed state as the capillary number is varied between 2 and 8, apparently because under these conditions a tendency for the droplets to widen in the vorticity direction counteracts their tendency to stretch in the flow direction. When a critical capillary number, Ca_c, is exceeded, the droplet finally stretches in the vorticity direction and forms a string which becomes thinner and finally breaks up, provided that the droplet elasticity is sufficiently high. For a fixed matrix shear stress and droplet elasticity, the steady-state deformation along the vorticity direction and the critical capillary number for breakup both increase with increasing viscosity ratio.

Keywords: Immiscible polymer blends; Droplet deformation and breakup; Steady shear flow

1. Introduction

Because of its importance in polymer processing, there has been considerable work on low Reynolds numbers shear-induced droplet deformation and breakup in blends of immiscible liquids, including blends of polymeric liquids. Taylor [17,18] predicted that for an isolated Newtonian droplet in steady simple shearing flow of a surrounding immiscible Newtonian fluid in the small-deformation limit, two dimensionless parameters control the droplet deformation behavior. The first parameter is the viscosity ratio between the two phases:

$$\eta_r = \eta_d/\eta_m \tag{1}$$

where η_d and η_m are the viscosities of the droplet phase and the matrix phase, respectively. The second dimensionless parameter is a capillary number, Ca:

$$\mathrm{Ca} = \frac{\eta_m \dot{\gamma} r_0}{\Gamma} \tag{2}$$

where $\dot{\gamma}$ is the applied shear rate, r_0 is the undeformed droplet radius, and Γ is the interfacial tension between dispersed and

* Corresponding author. Tel.: +66 2 218 4131; fax: +66 2 611 7221.
E-mail address: anuvat.s@chula.ac.th (A. Sirivat).

0032-3861/$ - see front matter © 2007 Elsevier Ltd. All rights reserved.
doi:10.1016/j.polymer.2007.04.020

matrix fluids. Taylor also predicted that the deformation parameter, Def, depends on Ca and η_r according to:

$$\mathrm{Def} \equiv \frac{a-b}{a+b} = \mathrm{Ca}\frac{19\eta_r + 16}{16\eta_r + 16} \tag{3}$$

where a and b are lengths of the major and minor axes of the deformed droplet, respectively. The capillary number is the ratio of the matrix viscous force ($\eta_m\dot{\gamma}$) to the interfacial stress (Γ/r_0). Correspondingly, for a given droplet and matrix fluid pair, there exists a critical capillary number, $\mathrm{Ca_c}$, at which the droplet ruptures in a flow field. For simple shear flow, the shape of the curve $\mathrm{Ca_c}$ vs. η_r is well known; at $\eta_r \approx 1$ Ca is minimized at $\mathrm{Ca_c} \cong 0.5$, while $\mathrm{Ca_c}$ becomes infinite at $\eta_r > 4$ so that droplets are stable at all capillary numbers [17,18,7,5]. Other correlations between $\mathrm{Ca_c}$ and η_r have also been reported [16,2].

The non-Newtonian viscoelastic behavior of common high-molecular weight polymer blends is expected to influence the droplet deformation and breakup. Working out a quantitative relationship between viscoelasticity and droplet deformation and breakup is a complicated task, because viscoelasticity is manifested in various ways, including first and second normal stress differences for both matrix and droplet fluids, and shear thinning in viscous and elastic properties of both fluids. Most experimental studies of droplet deformation and breakup with viscoelastic droplet and matrix fluids have been carried out with little or no systematic control that might allow the influence of one aspect of viscoelasticity to be assessed with others held fixed. However, from many experimental studies one can infer the general behavior that the elasticity of the droplet fluid inhibits droplet deformation causing the droplet to break at a higher capillary number, while elasticity of the matrix phase tends to destabilize the droplet causing it to break at a lower capillary number [5,6,19,12,13,10].

In an effort to better control the contributions of fluid viscoelasticity, some studies have chosen only one of the fluids (either matrix or droplet fluid) to be viscoelastic, with the other being Newtonian. Further control can be exerted by choosing for the viscoelastic fluid a so-called "Boger fluid," which is a weakly elastic dilute polymer solution in a Newtonian matrix. Boger fluids have the virtue of possessing little or no shear thinning in the shear viscosity and ideally also in the first normal stress coefficient. Studying a blend of a Boger fluid as the droplet phase in a Newtonian matrix fluid at a viscosity ratio of unity, Lerdwijitjarud et al. [10] found that $\mathrm{Ca_c}$ increased linearly with Wi_d up to a value of Wi_d of around unity, and thereafter approached an asymptotic value of around unity for high values of Wi_d. Here the dispersed-phase Weissenberg number, Wi_d, is defined as $Wi_d(\dot{\gamma}) \equiv [\Psi_{1d}(\dot{\gamma})/2\eta_d(\dot{\gamma})]\dot{\gamma}$, where $\Psi_{1d}(\dot{\gamma})$ is the first normal stress difference coefficient of the dispersed phase at an imposed shear rate $\dot{\gamma}$.

Studies with Boger fluids have generally only revealed rather modest effects of viscoelasticity on the deformation and breakup of droplets, relative to what is seen in Newtonian fluids. Namely one can observe a modest change (a factor of two or so) in $\mathrm{Ca_c}$, but the droplets deform in the flow direction to a similar degree as in blends of Newtonian droplet and matrix fluids. For highly elastic melts, very large increases are observed (more than a decade) in the capillary number required for droplet breakup. Moreover, for some melts, a new mode of droplet deformation, namely transient and steady-state droplet widening or elongation along the vorticity axis, has been observed for viscoelastic droplets sheared in viscoelastic matrices [11,9,15,14,4]. Experimental work showing this widening phenomenon was reviewed earlier [4]. Here it suffices to note that droplet widening has only been observed in blends containing viscoelastic melts, with one exception. Mighri and Huneault [14] studied the deformation and breakup mechanisms of droplets composed of viscoelastic Boger fluid in a Newtonian matrix (PDMS). At low shear rates, they found that the dispersed drop was oriented along the flow field and drop deformation increased with shear rate, as expected. However, when a critical shear rate was reached [$\mathrm{Ca_c} \approx 5.5$], the deformed drop began to contract in the flow direction. After increasing the shear rate above this critical value, drop contraction occurred, followed by elongation perpendicular to the flow direction. This elongation increased with shear rate until breakup occurred. In our studies with polybutadiene Boger fluids [10], we did not observe droplet widening over the range of Weissenberg numbers and capillary numbers we were able to access, despite using very high-molecular weight polybutadienes (M_w above one million) at concentrations high enough (1%) to produce significant shear thinning.

In an effort to access more significant effects of elasticity than could be obtained using Boger fluids, Cherdhirankorn et al. [4] studied blends of shear-thinning polymer melts, with properties and temperatures chosen to maintain the viscosity ratio near unity at the shear rates used. Viscoelastic modes of transient droplet deformation and droplet extension in the vorticity direction were reported for isolated droplets in two immiscible polymer blends (PS/HDPE) of equal viscosity in a simple shearing flow. In the blend with high elasticity of matrix and dispersed phases, the droplets initially deformed in the flow direction after startup of a steady shear but then began reverting to a spherical shape, and eventually deformed in the vorticity direction. In the second, low-elasticity system, the droplets first deformed in the shear direction, and thereafter continuously contracted in the flow direction until they reached their steady-state shapes. The droplets eventually deformed preferentially along the vorticity direction with increasing capillary number. Above a critical capillary number, breakup occurred whose mechanisms critically depended on the droplet elasticity.

The new work reported here extends the previous study of Cherdhirankorn et al. by considering the effect of the viscosity ratio, as well as capillary number and droplet elasticity on isolated droplet deformation and breakup. In addition, we want to find out if a blend system exists in which droplet deformation does not occur over a certain range of capillary number. Our earlier work [4] suggested that such behavior might be exhibited under conditions in which the tendency of the droplet to stretch in the flow direction due to viscous forces is balanced by a tendency to deform in the vorticity direction due to elasticity, leading to a state of almost no deformation over a range

of shear rates. Such a condition of shearing flow with no droplet deformation or breakup might be useful if spherical, or unusually large, droplets are desirable under a shearing flow, or might be a condition to avoid if the opposite is true.

2. Experiments

2.1. Materials

The materials used in this study are two grades of high-density polyethylene (HDPE1 and HDPE2) as the matrices. Three grades of polystyrene (PS1, PS2, and PS3) are used as the dispersed phases. The properties of all polymers are tabulated in Table 1. Polystyrene resins were prepared by crushing them into small pieces and their sizes were selected by passing the flakes though a 425 μm sieve. All polymers were heated at 80 °C under vacuum for 12 h to eliminate any volatile substances.

2.2. Rheological characterization

The steady-state shear viscosity and the first normal stress difference of each polymer were measured by a cone-and-plate rheometer (ARES, Rheometric Scientific) using a 25-mm diameter plate and a cone angle of 0.1 rad. Figs. 1 and 2 show rheological properties of the polymers chosen in our study. Four pairs of polymers and operating temperatures were chosen in our study. Table 2 lists the polymers and the four blend systems (A–D) investigated in this work, chosen to have viscosity ratios of somewhat greater than unity (2.6), less than unity (0.5), and unity. The interfacial tension values for the polymer blend systems were taken from Ref. [3]: 5.84 mN/m for System A at 143 °C, 5.60 mN/m for System B at 155 °C, 5.92 mN/m for System C at 139 °C, and 5.79 mN/m for System D at 147 °C. Since N_1 values for systems C and D were not accurately measurable, we used the relation $N_1 = 2G'$ at the frequency equal to the shear rate in order to calculate Wi_d and Wi_m.

2.3. Observation of an isolated droplet in shearing flow

2.3.1. Shearing apparatus

To generate a simple shear flow and to observe droplet behaviors, we used a commercial flow cell device (Linkam CSS 450, Linkam Scientific Instruments Ltd., UK) with two quartz parallel disks attached to an optical microscope (Leica DMRPX, Leica Imaging Systems Ltd.). The images were recorded by a CCD camera (Cohu 4910, Cohu Inc., USA). The obtained images were analyzed on a computer using the Scion image software (http://www.scioncorp.com).

Table 1
Properties of polymers used

Polymer	Suppliers	Grade	M_w
HDPE1	Bangkok Polyethylene	1600J	68,000[a]
HDPE2	Aldrich	Cat#42,801-9	46,000[a]
PS1	Polyscience	–	67,000[b]
PS2	Polyscience	Cat#18544	50,000[c]
PS3	Polyscience	Cat#23637	800–5000[c]

[a] Obtained from fitting zero-shear viscosity data with a 3.4-power correlation at 190 °C ($\eta_0 = 5.8 \times 10^{-14} M_w^{3.41}$) as reported by Arnett and Thomas [1].
[b] Measured by gel permeation chromatography based on polystyrene standard calibration.
[c] Quoted by the manufacturers.

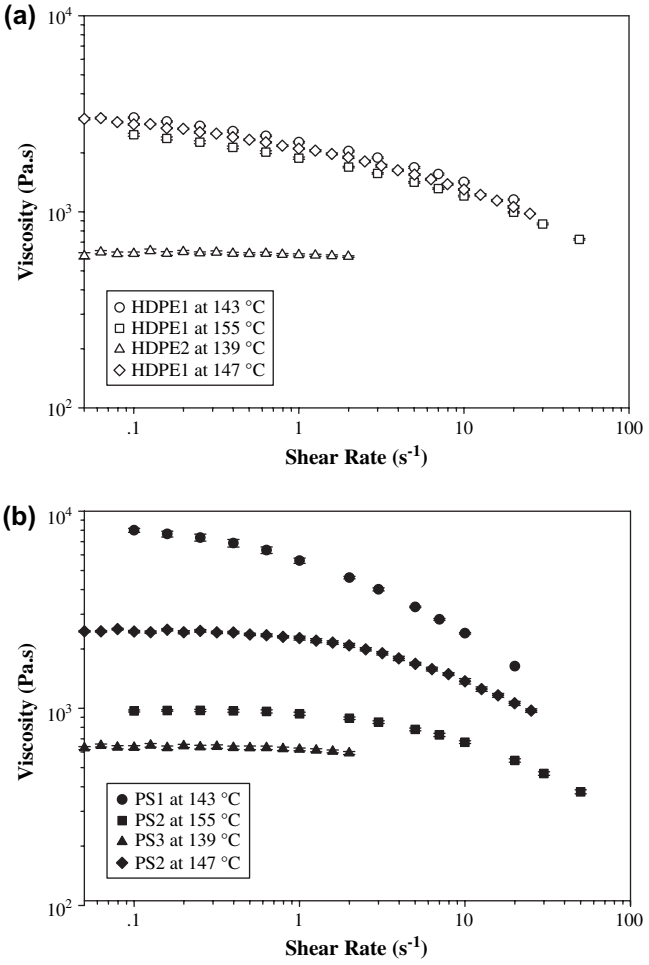

Fig. 1. Viscosity as a function of shear rate of the polymers at the temperatures in which the experiments were carried out: (a) matrix phases; (b) dispersed phases.

2.3.2. Sample preparation

HDPE was molded into a disk 25 mm in diameter and 0.5–1.0 mm in thickness by compression molding at 140 °C. To load PS droplets into the HDPE matrix, we used a pin to put a small amount of PS powder onto the HDPE disk, and then covered this with another HDPE disk to form a sandwich. The sandwich was then placed onto the bottom disk and covered with the top disk of the flow cell. The sample was held at the testing temperature until complete melting occurred.

2.3.3. Optical microscopy of isolated droplets

Droplet deformation and subsequent relaxation from its deformed ellipsoidal shape were observed using an optical microscope at a magnification that depended on the droplet

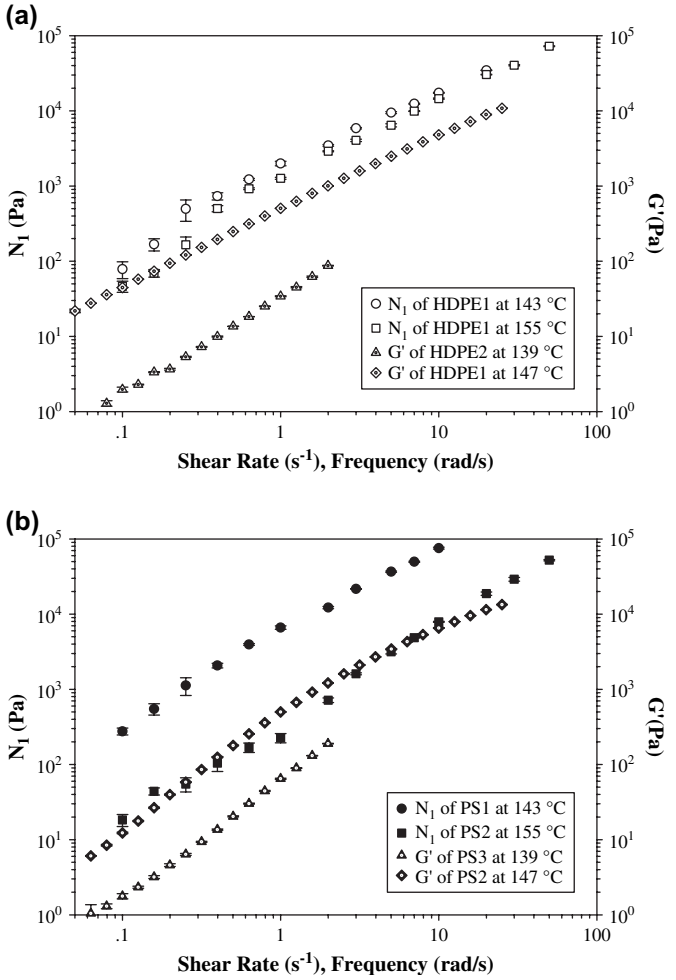

Fig. 2. The first normal stress difference, N_1, vs. shear rate and the storage modulus, G', vs. frequency for the polymers at the temperatures in which the experiments were carried out: (a) matrix phases; (b) dispersed phases.

size. Around 100–200 droplet images were recorded (10–20 s per frame).

Since the images of the deformed droplet were captured only in the plane perpendicular to the shear gradient direction, the true length of the major principle axes of the ellipsoidal droplet could not be determined directly. The lengths of all three principle axes can, however, be calculated from a planar image using the known droplet volume provided that we know the orientation angle (θ), i.e., the angle between the major axis and the flow direction. Lacking this orientation angle, we followed our earlier work [4] and used the apparent observable lengths of the principle axes to describe the behavior of each droplet by defining a modified deformation parameter Def*:

$$\mathrm{Def}^* = (a^* - c)/(a^* + c) \tag{4}$$

where the asterisk indicates that the deformation parameter is an apparent one obtained from the droplet image projected into the flow-vorticity plane (see Fig. 3) [8].

Table 2
Polymer blend systems investigated

Blend system	Blend components (droplet/matrix)	Temperature (°C)	Viscosity ratio (η_d/η_m)
A	PS1/HDPE1	143	2.6
B	PS2/HDPE1	155	0.5
C	PS3/HDPE2	139	1.0
D	PS2/HDPE1	147	1.0

System D is System A of Cherdhirankorn et al. [4].

2.3.4. Transient deformation

Due to the limitation of the flow cell, a single droplet cannot be observed continuously from startup until it attains a steady-state shape, since this droplet will move out of the viewing plane after imposing a given strain. Since the behavior of a given isolated droplet is assumed to be reproducible, the complete transient deformation history of an isolated droplet of a particular size was determined, as before [4], by combining the results of several experiments with the droplets of nearly equal sizes. In the experiment of type 1, the droplet was moved out of the viewing window by imposing a strain, typically less than 40 strain units ($\approx$1 orbit). The droplet was then left to relax for at least 60 min. Then the isolated droplet was deformed at the required strain rate for the same strain but in the opposite direction until it moved back into the viewing window where we could image its deformation. In experiments of type 2, the droplet was deformed continuously at a fixed shear rate and images of the droplet were taken whenever the droplet passed through the viewing window. To obtain clear droplet images, we stopped the flow each time the droplet appeared within the viewing window for a period of less than 1 s and an image was taken. This time interval was sufficiently small enough to avoid droplet relaxation; the typical transient time scale for droplet relaxation in our experiments was of order 10^3 s. Then, the flow was initiated again until the droplet passed through the viewing window again. By repeating this procedure, we could assemble a history of deformation from

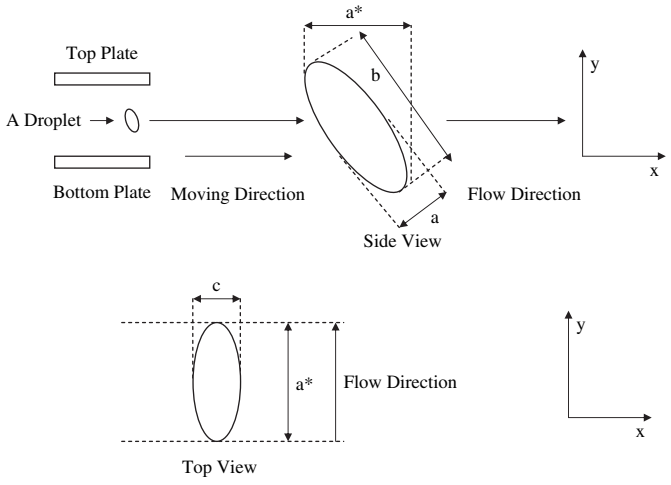

Fig. 3. Schematic drawing of a single drop observed from the side and top views of the optical microscope; a and b are the long and short axes of the droplet in the flow-radial plane, a^*, the "apparent axis" is the droplet length projected into the flow direction, and c is the principal axis in the radial direction.

the initial time to the time at which the droplet attained its steady-state shape. The imposed values of capillary number, Ca, were chosen to be 5, 8, and 11 by using droplets of various sizes at a fixed shear rate of 0.4 s^{-1}. To separate the effects of viscous forces from those of elasticity, some experiments were carried out with the capillary number, Ca, held fixed. The elastic force was varied by changing the shear rate, $\dot{\gamma}$, from 0.10, to 0.17, to 0.40, to 0.63 s^{-1} and the corresponding droplet size, $2r_o$, was varied inversely with the shear rate from 290, to 177, to 85, to 56 μm, respectively, so that $Ca = \eta_m \dot{\gamma} r_0 / \Gamma$ was fixed at 8.

2.3.5. Steady-state deformation and breakup

Here, we describe the procedure used to obtain the steady-state shapes of isolated droplets below the critical capillary number for breakup. Generally, the strain required to reach a steady-state droplet shape increases with the droplet size. From several transient experiments, the required strain to reach steady-state droplet shape was found to be approximately 4000 strain units. Therefore a constant shear rate was applied until a strain exceeding 4000 strain units was attained. To ensure that the steady-state deformation had indeed been attained, when a selected droplet passed through the viewing window, the droplet was imaged many times over a period of 5–10 min and Def* was measured and determined until its value became constant. Subsequently, the flow was stopped and the droplet shape relaxation was recorded with the CCD camera at speeds of 10–20 s per frame for approximately 90 min.

The critical capillary number was determined by finding the smallest droplet size at which drop breakup was observed at a fixed shearing rate of 0.4 s^{-1} for Systems A and C, and of 0.63 s^{-1} for System B.

For droplets for which no steady-state shape was obtained, the unstable shapes of the droplets were recorded until the droplets broke. The breakup process for System A was studied at a fixed capillary number Ca equal to 11 using a shear rate of 0.40 s^{-1}; and for System B, we selected Ca value of 9.5 with shear rates of 0.20 and 0.63 s^{-1}. These shear rates or capillary numbers were slightly above the minimum values needed to achieve breakup for these systems.

Our experiments were carried out at shear rates at which the viscosities and first normal stress coefficients were mildly shear thinning, so the capillary number and Weissenberg number were calculated using the actual viscosity and first normal stress difference at which the experiments were performed.

3. Results and discussion

Fig. 4a shows a sequence of optical images during the transient droplet deformation for blend System A, with $\eta_r = 2.6$, $Ca \approx 8$ and $Wi_d \approx 0.15$. Here, the drop stretches at first along the flow direction and later along the vorticity direction. It nearly recovers its spherical shape at a time of around 6000 s before it stretches again along the flow direction. Finally, it attains its steady-state shape by contracting along the flow direction and stretching along the vorticity direction.

3.1. Transient deformation in steady shear flow

3.1.1. Effect of capillary number

Here we describe the effect of imposed capillary number, Ca, on the transient droplet deformation, over a strain period between 40 and 4000 for blend System A. The conditions of the experiment are: a fixed shear rate of 0.4 s^{-1}, a fixed Weissenberg number, Wi_d, of 0.38, a fixed viscosity ratio of 2.6, and imposed capillary numbers, Ca, of 5, 8, and 11 obtained by choosing droplets of sizes equal to 52 (±5), 85 (±5), and 125 (±7) μm, respectively. The parameters of these experiments are tabulated in Table 3.

Fig. 5a displays the transient deformation parameter Def* vs. strain between 40 and 4000 at three capillary numbers: 5, 8, and 11. In these experiments, we can divide the deformation evolution into three regimes. Def* initially decreases towards a local negative minimum at a strain of around 300, in which its amplitude depends on Ca. In the second regime, 300 < strain < 900, Def* increases towards a local maximum whose value is close to zero, or the state of no deformation, at a strain of approximately 900. For strains > 900, Def* decreases and becomes negative until attaining its steady-state negative value which depends on Ca: $Def^*_{ss} = -0.065$ and -0.205 for $Ca \approx 5$ and 8, respectively. In the experiment with $Ca \approx 11$, Def* eventually decreases to a value of -0.8 before breakup occurs, and therefore Def^*_{ss} does not exist at or above this capillary number. Qualitatively similar oscillations in droplet deformation were reported in our earlier work [4]. We believe that these oscillations may result from tumbling of the deformed droplet in the shear flow.

Fig. 5b and c shows the corresponding evolution of a^*/D_o and c/D_o vs. strain between 40 and 4000. In the first regime, in which 40 < strain < 300, a^*/D_o first increases above unity and then decreases towards a local minimum of less than unity at a strain of 300. In this regime, there is an initial weak flow elongation followed by a shrinkage of the major principle axis to a value below its initial value. In the second regime with 300 < strain < 900, a^*/D_o increases again towards a local maximum whose amplitude depends on Ca at a strain of 900. In the third regime, where strain > 900, a^*/D_o decreases towards its steady-state value equal to 0.96 for both $Ca \approx 5$ and 8, or towards its final value of 0.4 before drop breakup at $Ca \approx 11$. In the first regime, the deformation c/D_o along the vorticity axis initially rises to a local maximum whose amplitude depends on Ca at a strain of 300. The stretching along the vorticity direction in this regime coincides with the initial period in which the major principle axis goes through an overshoot and shrinks. In the second regime, c/D_o decreases slightly and then monotonically rises towards its steady-state values of 1.09 and 1.34 for $Ca \approx 5$ and 8, respectively. For $Ca \approx 11$, the final value of c/D_o before breakup is equal to 5.2 at the strain of 4073. In summary, the evolution of the droplet deformation with time can generally be divided into three regimes. In the first regime, there is a weak flow elongation followed by a complete recovery along with a slight stretching in the vorticity direction. In the second regime, a flow elongation reappears along with a slight contraction

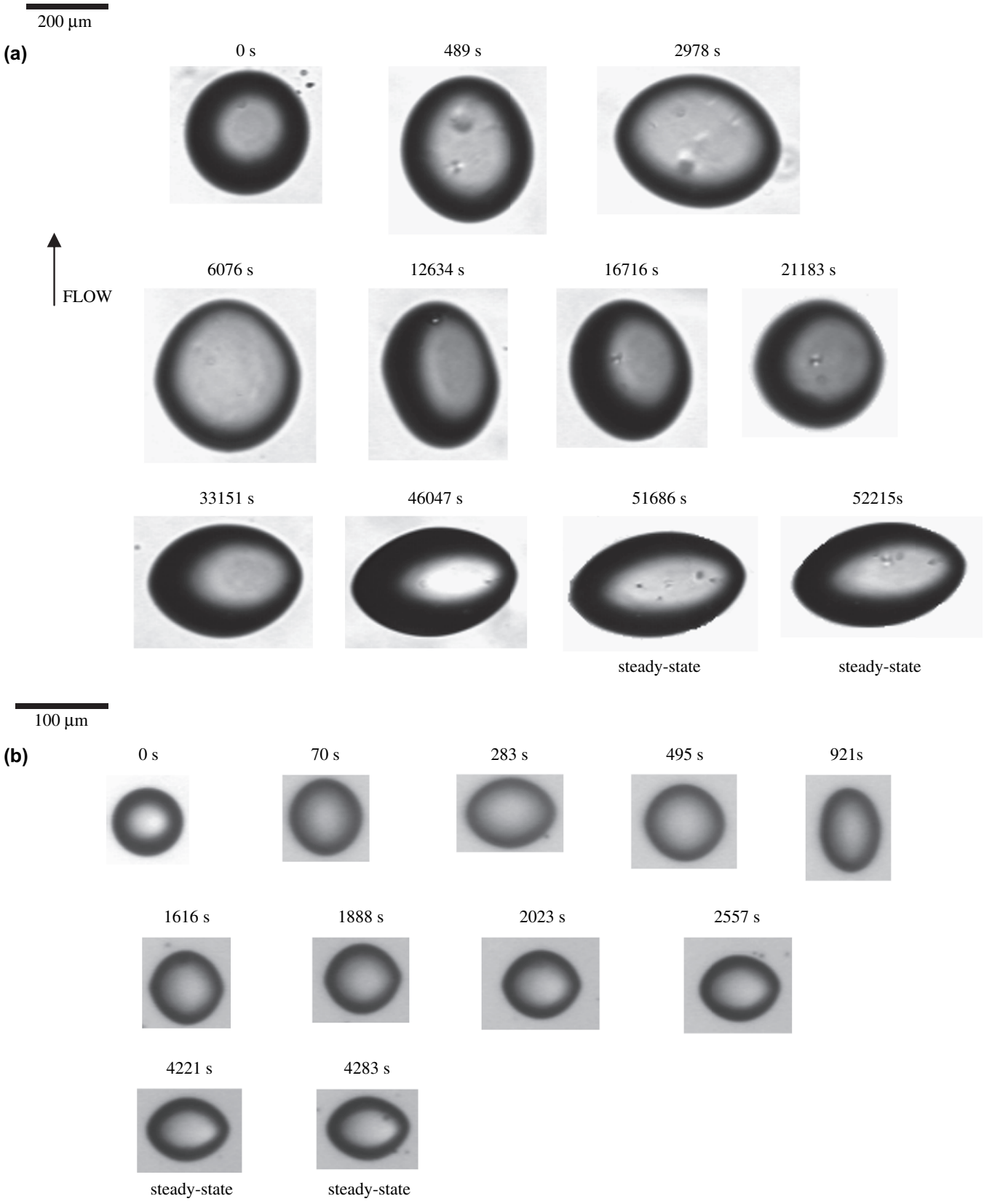

Fig. 4. Sequence of images of deforming isolated droplets after startup of a steady shear at fixed Ca ≈ 8 and Wi_d ≈ 0.15. (a) System A: $\eta_r = 2.6$, a shear rate of 0.1 s^{-1}, and $D_o = 86$ μm; (b) System B: $\eta_r = 0.5$, a shear rate of 0.63 s^{-1}, and $D_o = 72$ μm.

Table 3
Experimental parameters for Fig. 5, blend System A (PS1/HDPE1), at a shear rate of 0.4 s^{-1}, $Wi_d = 0.38$, and Ca = 5, 8, and 11 obtained by varying the initial droplet size: $d_o \approx 52$, 85, and 125 μm; and for Fig. 6: blend System A (PS1/HDPE1), Ca ≈ 8, $Wi_d = 0.24$, 0.38 and 0.49 obtained by varying the shear rate, $\dot{\gamma} =$ 0.17, 0.40–0.63 s^{-1}

Data	Shear rate (s^{-1})		
	0.17	0.40	0.63
Temperature (°C)	143	143	143
η_d: viscosity of the droplet phase (Pa s)	7620	6880	6340
η_m: viscosity of the matrix phase (Pa s)	2870	2580	2440
η_r: viscosity ratio	2.6	2.6	2.6
Γ: interfacial tension (mN/m)	5.84	5.84	5.84
$N_{1,d}$: first normal stress difference of the droplet phase (Pa)	620	2080	3950
$N_{1,m}$: first normal stress difference of the matrix phase (Pa)	208	733	1230
$N_{1,r}$: first normal stress difference ratio	2.97	2.84	3.21
Ca: capillary number	≈8[a]	≈5, 8, 11[a]	≈8[a]
D_o: initial droplet size (μm)	177	52, 85, 125	56
Wi_d: Weissenberg number of the dispersed phase	0.24[b]	0.38[b]	0.49[b]
Wi_m: Weissenberg number of the matrix phase	0.21[c]	0.36[c]	0.40[c]

[a] $Ca = D_0\dot{\gamma}\eta_m/2\Gamma$.
[b] $Wi_d = N_{1,d}/(2\eta_d\dot{\gamma})$.
[c] $Wi_m = N_{1,m}/(2\eta_m\dot{\gamma})$.

in the vorticity direction. In the third regime, a contraction occurs in the flow direction along with continuous stretching along the vorticity direction until the droplet attains a steady-state condition in which Def^*_{ss} is less than zero. The critical capillary number for System A is approximately equal to 11.

3.1.2. Effect of elasticity

Next we investigate the influence of the droplet elasticity on the droplet transient deformation. We focus again on System A, whose viscosity ratio was 2.6, and fix the capillary number Ca at around 8.0. Using shear rates given in Table 3 we vary the droplet Weissenberg number over a range of

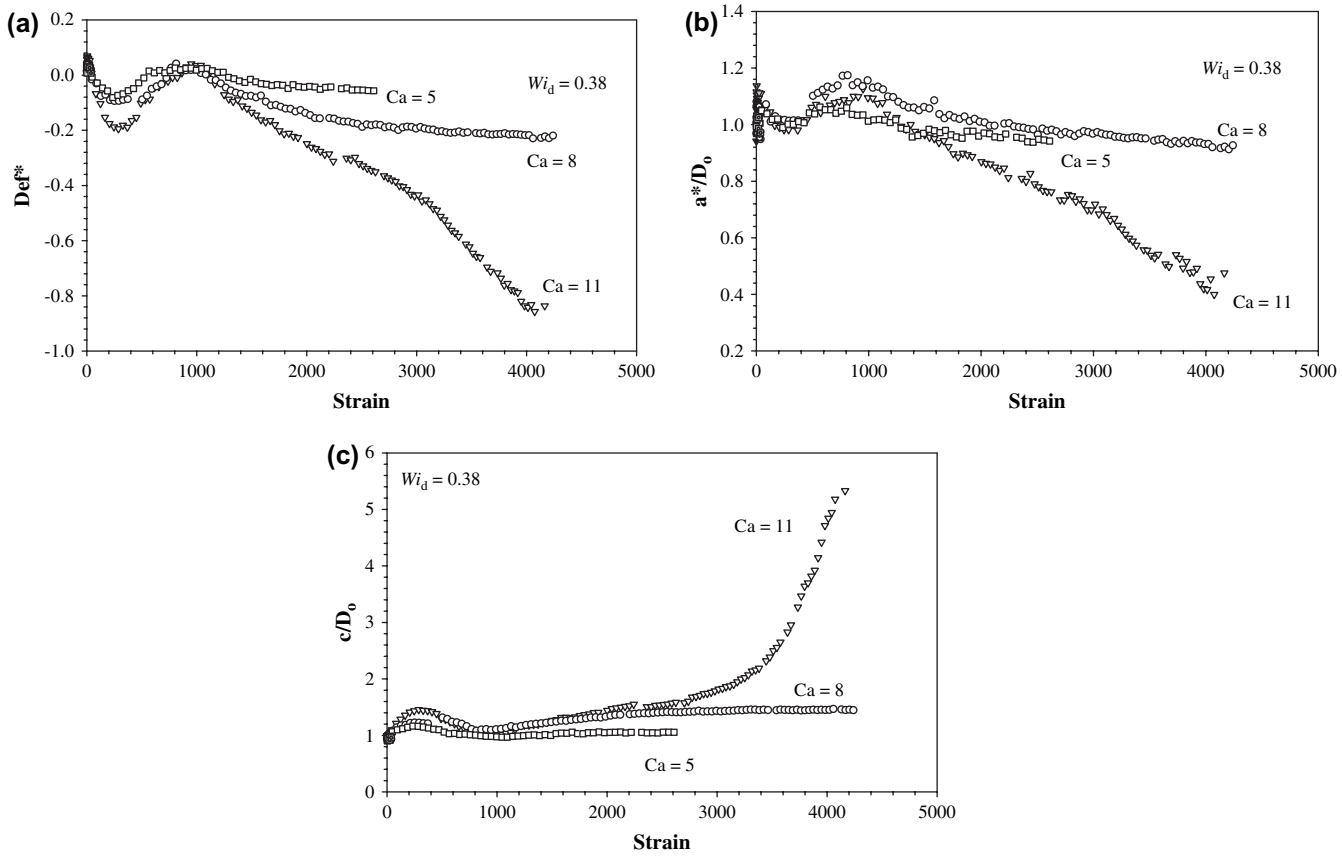

Fig. 5. Transient deformation of isolated droplets of System A vs. strain at a shear rate of 0.4 s^{-1}, $Wi_d = 0.38$, and at various Ca values: Ca ≈ 5, with initial droplet diameter $D_o = 52$ μm (□); Ca ≈ 8, $D_o = 85$ μm (○); Ca ≈ 11, $D_o = 125$ μm (▽). (a) Def* vs. strain; (b) a^*/D_o vs. strain; and (c) c/D_o vs. strain.

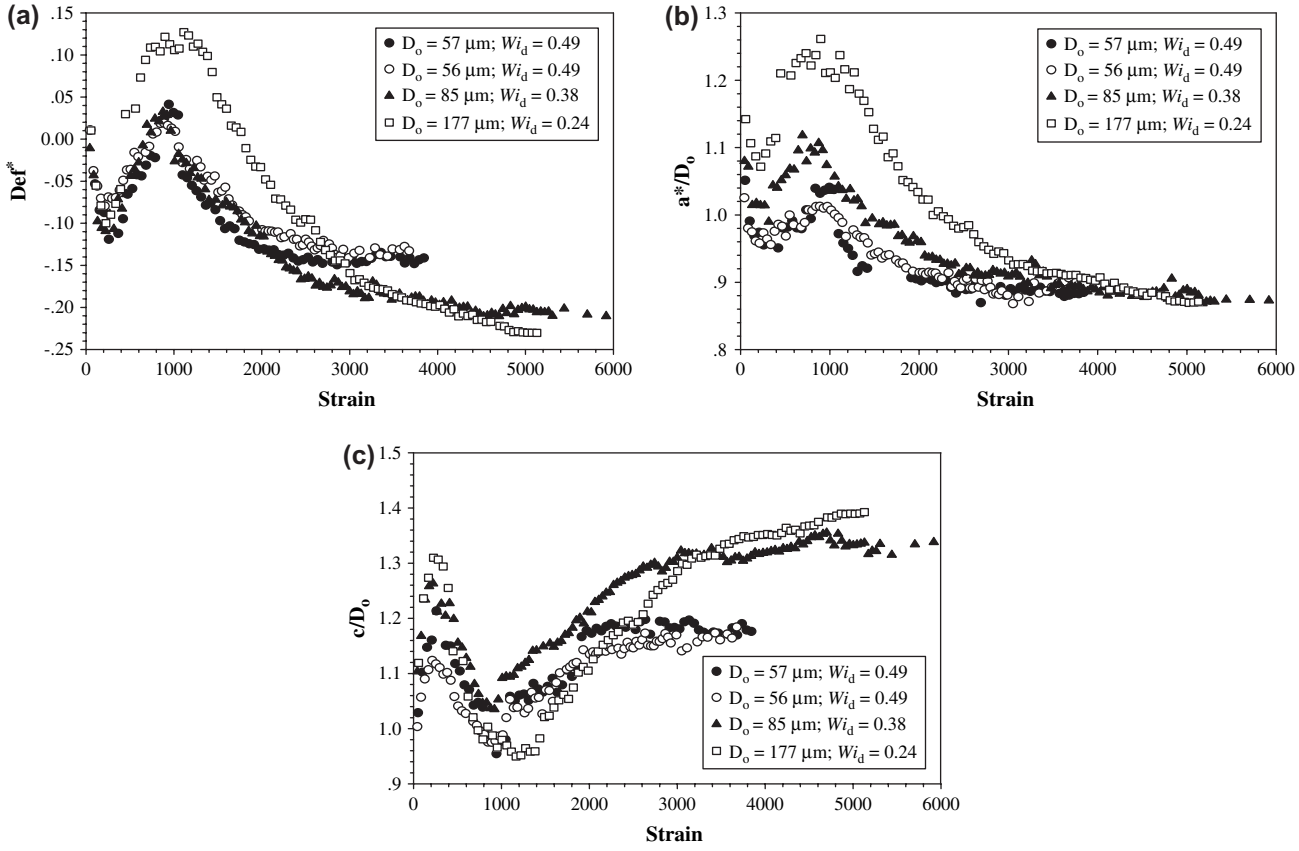

Fig. 6. Transient deformation of isolated droplets of System A vs. strain at fixed Ca ≈ 8, at various shear rates: $\dot{\gamma} = 0.63\ s^{-1}$, $Wi_d = 0.49$ with $D_o = 57\ \mu m$ (●) and 56 μm (○); $\dot{\gamma} = 0.4\ s^{-1}$, $Wi_d = 0.38$ with $D_o = 85\ \mu m$ (▲); $\dot{\gamma} = 0.17\ s^{-1}$, $Wi_d = 0.24$, $D_o = 177\ \mu m$ (□). (a) Def* vs. strain; (b) a^*/D_o vs. strain; and (c) c/D_o vs. strain.

around 0.25–0.5, keeping Ca fixed at around 8.0 by choosing droplet sizes that vary inversely with the shear rate.

In Fig. 6a, the evolution of Def* vs. strain again shows three regimes of transient deformation. With increasing Wi_d, the positive maximum in Def* at a strain of around 1000 decreases and the steady-state negative Def* increases, i.e., becomes less negative. Fig. 6b and c shows the corresponding evolution of a^*/D_o and c/D_o with strain. Note in Fig. 6c that the steady-state value of c/D_o decreases with increasing Wi_d, i.e., the droplet widening is diminished.

Table 4
Experimental parameters for Figs. 7 and 8

Data	Blend system (drop/matrix)			
	System A (PS1/HDPE1)	System B (PS2/HDPE1)	System C (PS3/HDPE2)	System D (PS2/HDPE1)
Temperature (°C)	143	155	139	147
Shear rate (s^{-1})	0.10	0.63	0.40	0.50
η_d: viscosity of the droplet phase (Pa s)	7996	964	630	2323
η_m: viscosity of the matrix phase (Pa s)	3026	2013	595	2331
η_r: viscosity ratio	2.6	0.5	1.0	1.0
Γ: interfacial tension (mN/m)	5.84	5.60	5.92	5.79
$N_{1,d}$: first normal stress difference of the droplet phase (Pa)	276	168	–	–
$N_{1,m}$: first normal stress difference of the matrix phase (Pa)	78.3	920	–	834
$N_{1,r}$: first normal stress difference ratio	3.53	0.18	–	–
G'_d: storage modulus of the droplet phase (Pa)	–	–	≈13	179
G'_m: storage modulus of the matrix phase (Pa)	–	–	≈10	248
G'_r: storage modulus ratio	–	–	1.0	0.72
Wi_d: Weissenberg number of the dispersed phase	0.17	0.14	≈0.05	0.15
Wi_m: Weissenberg number of the matrix phase	0.13	0.36	≈0.04	0.36
D_o (μm)	150–370	25–80	100–400	28–90

$Wi_d = N_{1,d}/(2\eta_d\dot{\gamma})$ or $G'_d/(\eta_d\dot{\gamma})$; $Wi_m = N_{1,m}/(2\eta_m\dot{\gamma})$ or $G'_m/(\eta_m\dot{\gamma})$.

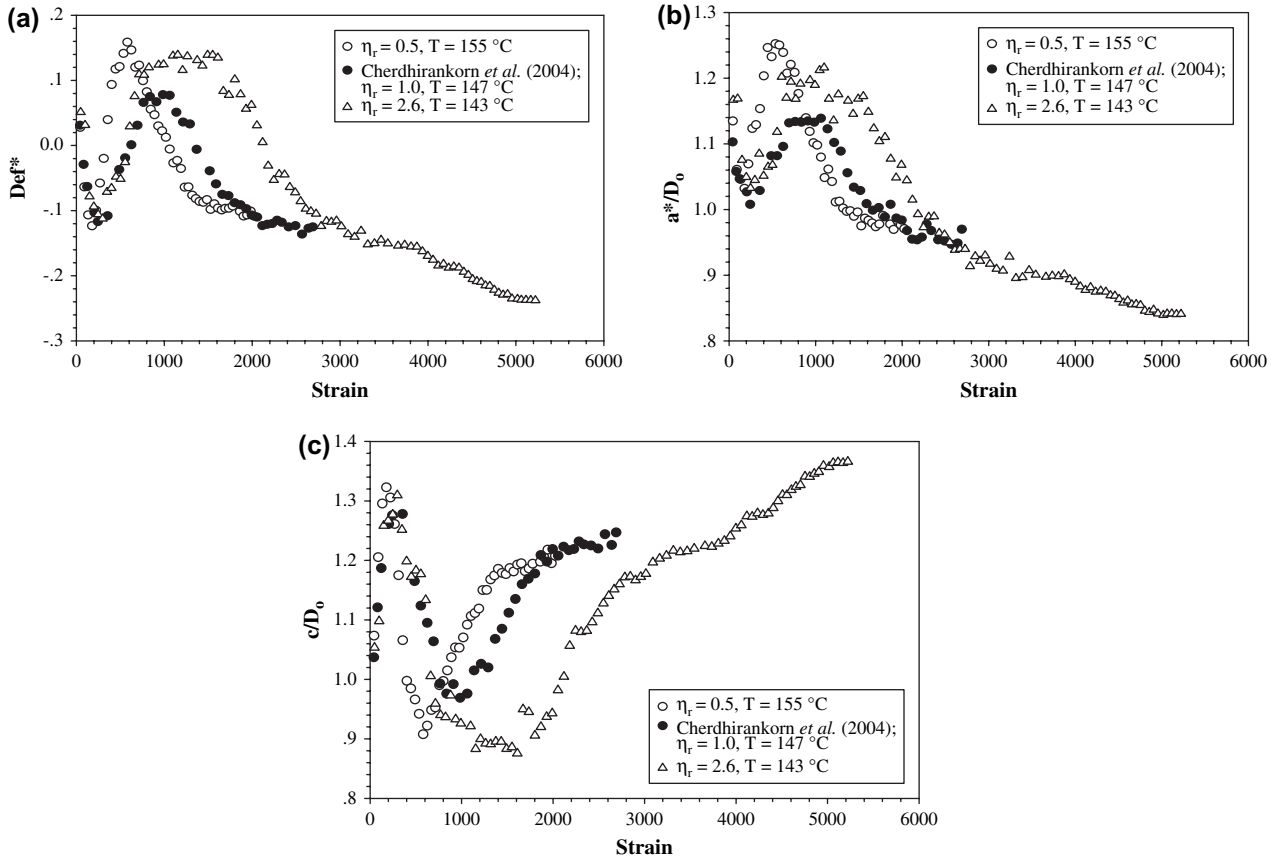

Fig. 7. Transient deformation of isolated droplets of Systems A, B and D vs. strain at fixed Ca ≈ 8 and $Wi_d \approx 0.15$: $\eta_r = 0.5$, $\dot{\gamma} = 0.63\ s^{-1}$ (○); $\eta_r = 1.0$, $\dot{\gamma} = 0.50\ s^{-1}$ (●); $\eta_r = 2.6$, $\dot{\gamma} = 0.4\ s^{-1}$ (△). (a) Def* vs. strain; (b) a^*/D_o vs. strain; and (c) c/D_o vs. strain.

3.1.3. Effect of viscosity ratio

To investigate the effect of viscosity ratio on droplet transient deformation, Systems B, D, and A, with viscosity ratios of 0.5, 1.0, and 2.6, respectively, were investigated at a capillary number, Ca, fixed at 8.0 and Weissenberg number, Wi_d, fixed at around 0.15, see Table 4. Fig. 7a shows that the magnitudes of the local minimum and maximum of Def* are insensitive to viscosity ratio for these systems, but the local maximum shifts to larger strains with higher viscosity ratio, indicating a slower tumbling with increased viscosity ratio, probably as a result of slower deformation of the more viscous droplet fluid. The steady-state value of Def^*_{ss} becomes more negative with increased viscosity ratio. Fig. 7b and c shows the corresponding evolution of a^*/D_o and c/D_o. Comparing optical images in Fig. 4a and b, it is evident that the system with lower viscosity (Fig. 4b with viscosity ratio of 0.5) reaches steady state faster than that for the higher viscosity ratio (Fig. 4a with viscosity ratio of unity).

3.2. Steady-state deformation

Fig. 8 shows the steady-state values of Def* vs. Ca for Systems A–D, corresponding to viscosity ratios of 2.6, 0.5, 1.0, and 1.0, respectively. In these systems, the droplet Weissenberg number, Wi_d, was fixed at 0.17, 0.14, 0.05, and 0.15, respectively, for each of these systems, with Ca varied by varying droplet size, see Table 4. It is evident that Def^*_{ss} becomes increasingly negative with increasing Ca and with increasing viscosity ratio, η_r. On the other hand, for Systems C and D with the same viscosity ratio equal to 1, we find that Def^*_{ss} becomes more negative with increasing Wi_d. Therefore, droplet elasticity appears to be necessary for droplets to stretch along the

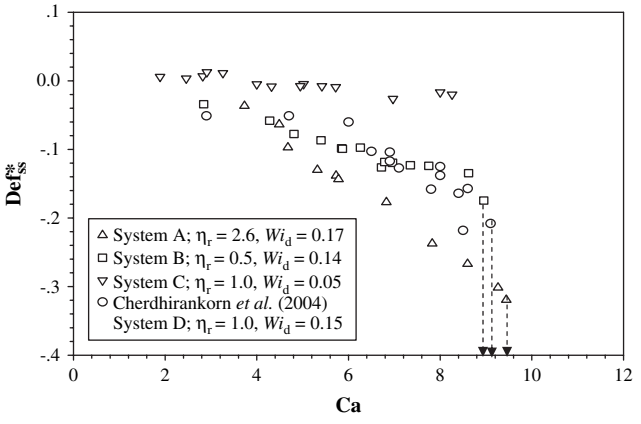

Fig. 8. Steady-state deformation parameters vs. capillary number. For $Wi_d \approx 0.15$, △ – System A with $\eta_r = 2.6$ at a shear rate of $0.1\ s^{-1}$ (△); System D of Cherdhirankorn et al. [4] with $\eta_r = 1.0$ at a shear rate of $0.5\ s^{-1}$ (○); and System B with $\eta_r = 0.5$ at a shear rate of $0.63\ s^{-1}$ (□). For $Wi_d \approx 0.05$, ▽ – System C, with $\eta_r = 1.0$, and a shear rate of $0.4\ s^{-1}$ (▽). Arrows indicate Ca_c of Systems A, B, and D.

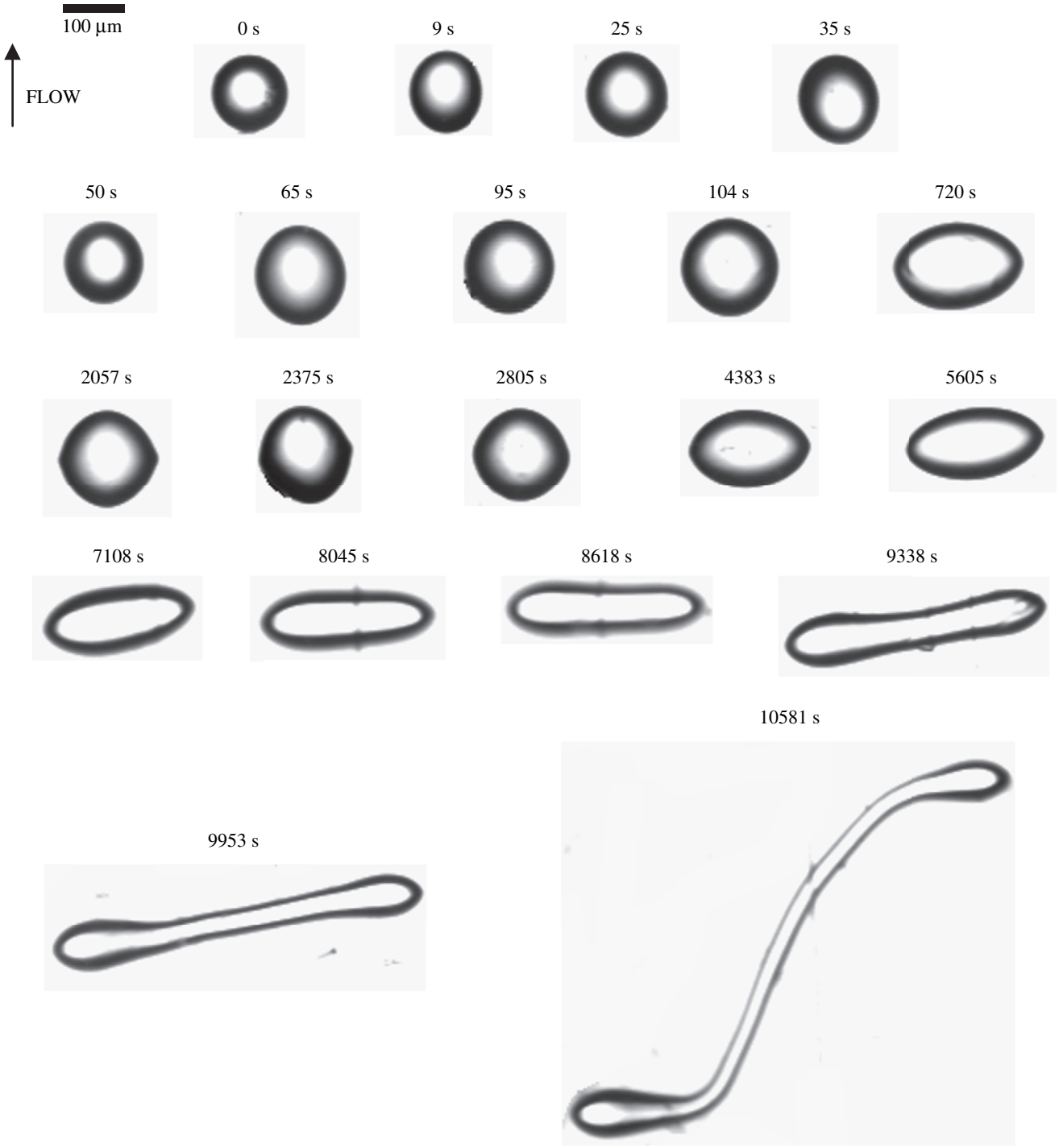

Fig. 9. Sequence of images of droplet breakup for System A: a shear rate of 0.40 s^{-1}, $D_o = 125$ (±7) μm, $Wi_d = 0.38$, $\eta_r = 2.6$, and Ca = 11.

vorticity direction, but the viscosity ratio also influences the magnitude of the stretching in the vorticity direction. Finally, it is interesting to note that the steady-state values of Def^*_{ss} for System C are quite close to zero and vary slightly as Ca increases from 2 to 8. Thus, it is possible to choose a material system with a fixed viscosity ratio with a corresponding low Wi_d (0.05) value such that droplets do not deform at steady shear rates over a range of values of Ca. For Newtonian fluids (for which $Wi_d = Wi_m = 0$), for $\eta_r = 1$ Def^*_{ss} rises with Ca to a value of around 0.5 at Ca ≈ 0.5, after which breakup occurs. Thus, even for Wi_d as low as 0.05, droplet deformation in these melts deviates considerably from that in Newtonian fluids. This latter result is an extremely peculiar one. System C is a blend of PS3 in HDPE2. According to Fig. 1, both of these melts have nearly flat, Newtonian, viscosities well beyond the shear rate of 0.4 s^{-1} at which the experiments reported in Fig. 8 were carried out. Both of these melts have shear stresses of around 230 Pa and first normal stress differences of around 20 Pa at this shear rate. Thus, it is surprising that there is such a large effect of such a small elasticity on both the steady-state deformation

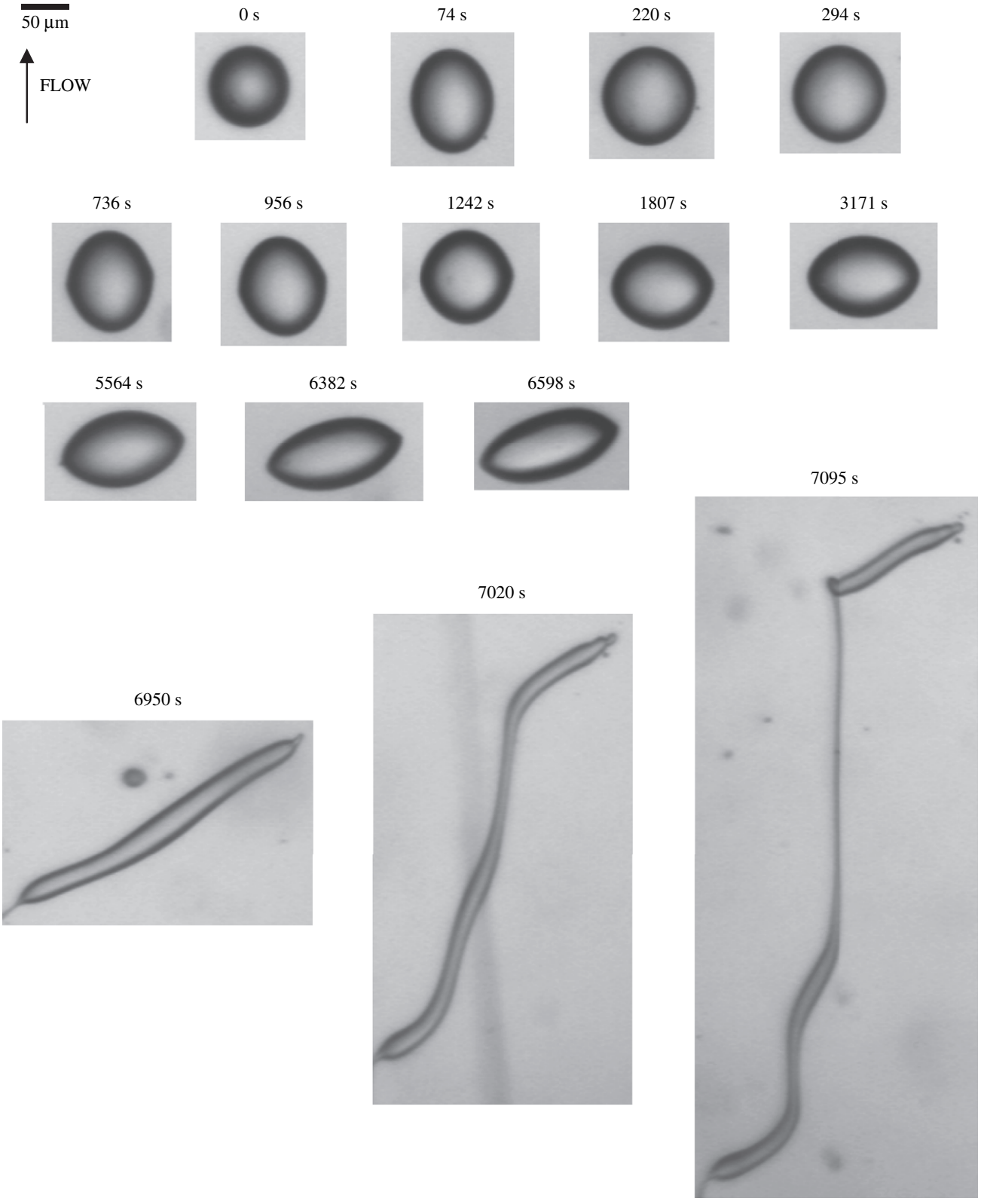

Fig. 10. Sequence of images of droplet breakup for System B: a shear rate of 0.63 s^{-1}, $D_o = 82$ μm, $Wi_d = 0.14$ for $\eta_r = 0.5$, and $Ca = 9.5$.

and the critical capillary number for breakup. Blends in which the droplet fluid was a Boger fluid with a higher first normal stress difference than that of PS3 nevertheless showed a much weaker effect of elasticity on droplet deformation [10]. A difference between the Boger fluid blends and those studied here that might account for this is that in the Boger fluid blends, the matrix fluid had much smaller first normal stress difference than the droplet fluid while in blend C studied here, the first

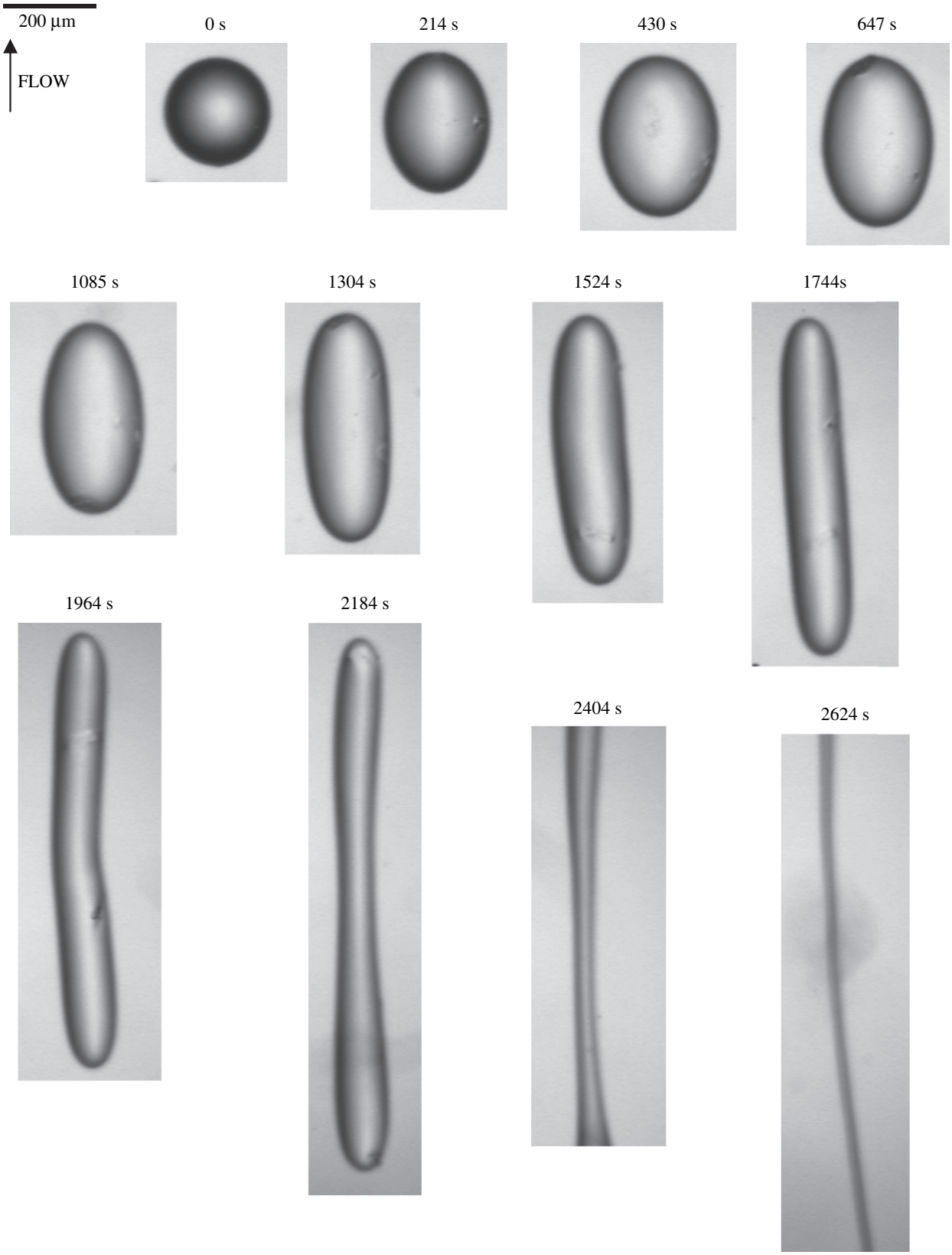

Fig. 11. Sequence of images of droplet backup for System B at a shear rate of 0.20 s^{-1}, $D_o = 225$ µm, $Wi_d = 0.25$, $\eta_r = 0.5$, Ca = 9.5.

normal stress differences, while small, were nearly equal for the droplet and matrix fluid. There are also likely to be differences in the second normal stress difference between the melts studied here and Boger fluids. However, these results show how sensitive droplet deformation is to the rheological properties of the fluids.

3.3. The critical capillary number

The critical capillary numbers for droplet breakup, Ca_c, were found to decrease modestly from around 10 to around 9 with viscosity ratio decreasing from 2.6 to 1.0 to 0.5 for Systems A, D, and B, respectively, which have viscosity ratios, η_r, of 2.6, 1.0, and 0.5; in each case Wi_d was around 0.15, and critical Def^*_c values were 0.40, −0.27, and −0.18, respectively. For Newtonian fluids, experimental Ca_c values are 0.5 [7], close to the predicted values [17,18]. We were unable to observe the breakup of System C, presumably because the steady-state deformation of this system is very small at the shear rates we could access.

3.4. Droplet breakup mechanism

The droplet breakup sequences of Systems A and B are shown in Figs. 9–11. The shear rate applied to System A was 0.40 s^{-1}, Ca ≈ 11 (slightly above Ca_c) and $Wi_d = 0.38$. For System B, the shear rate used was 0.63 s^{-1}, Ca ≈ 9.5 (slightly above Ca_c) and $Wi_d = 0.14$. We can see that in both systems, with $\eta_r = 2.6$ and 0.5 under these experimental conditions, the droplets follow oscillation patterns described previously, and eventually breakup along the vorticity direction. An S shape appears as the final droplet shape before breakup. This S shape presumably arises from the velocity gradient along the radial direction. A minor difference between the breakup patterns of Systems A and B is that, for System B whose viscosity ratio is smaller ($\eta_r = 0.5$), there is a more pronounced stretching along the flow direction.

4. Conclusions and perspective

We reported the transient droplet deformation, under startup of a steady shear flow, for viscoelastic melt blends with viscosity ratios ranging from 0.5 to 2.6. The evolution of droplet deformation, Def*, with time can be divided into three regimes: an initial flow elongation followed by contraction, a secondary flow elongation, and a final stretching along the vorticity direction. The magnitudes of the transient maxima and minima of Def* depend on Ca and Wi_d; but the period depends mostly on η_r. For the elastic melt components studied here, the steady-state deformation parameter, Def^*_{ss}, becomes more negative with increasing Ca, and with increasing Wi_d and η_r at fixed Ca. For η_r fixed at unity, we were able to find an experimental condition, with $Wi_d \approx 0.05$, at which droplets do not deform at steady state, for Ca values ranging up to 8. Droplets breakup along the vorticity direction if Wi_d is sufficiently high.

We also note that the critical value of the capillary number for breakup in the vorticity direction is high, around 8 in our experiments on elastic melt components. As noted in Section 1, for Newtonian fluids, the critical capillary number for breakup in the flow direction is around 0.5, and for weakly elastic droplet fluids with viscosity ratio of unity, this critical capillary number increases to around unity as the dispersed-phase Weissenberg number increases to unity. For our melts, and those of Hobbie and Migler [9], and the solutions of Migler [15], and Mighri and Huneault [14], droplet deformation in the vorticity direction is observed and breakup occurs at a much higher critical capillary number, around five or higher. Thus, it appears that viscoelasticity of the droplet phase impedes deformation and breakup in the flow direction. Elasticity of the droplet and/or matrix phase, if strong enough, can completely block breakup in the flow direction by inducing deformation in the vorticity direction. In this case, breakup can be deferred to much higher capillary numbers, around five or higher.

The conditions required to produce droplet elongation in the vorticity direction are still unclear. For some droplet fluids consisting of dilute or semi-dilute solutions of polymers in a Newtonian matrix (i.e., ''Boger fluids''), droplet Weissenberg numbers as high as unity can be reached with no droplet widening, while for the melts studied here, droplet widening is evident for Weissenberg numbers as low as 0.5, and droplet deformation in the flow direction is impeded for one system with a droplet Weissenberg number as low as 0.05, which differs strongly from earlier studies in which the droplet fluid was a Boger fluid. Thus, it seems clear that the droplet Weissenberg number is not the only, or even the most important, variable controlling droplet vorticity stretching. Our studies indicate that the viscosity ratio plays a role, and there have been suggestions in the literature [11,9,15,14] that the difference in first normal stress difference between the droplet and matrix fluids is important, as are the second normal stress differences of matrix and droplet fluids. To resolve this issue, fluids must be formulated with controlled first and second normal stress differences. Simulations of droplet deformation for viscoelastic droplet and matrix fluids would also help resolve this puzzle. Eventually, correlations of droplet vorticity stretching and breakup with the viscoelastic properties of the fluids are needed so that blends with desired droplet deformation and breakup characteristics can be designed.

Acknowledgements

A.S. would like to acknowledge supports from the Petroleum Petrochemical and Advanced Polymers Consortium, the Conductive and Electroactive Polymers Research Unit (Ratchadapiseksompoch, Chulalongkorn University), and the Thailand Research Fund (TRF), grant no. BRG4680015.

References

[1] Arnett RL, Thomas CP. J Phys Chem 1980;84:649–52.
[2] Bentley BJ, Leal LG. J Fluid Mech 1986;167:241–83.
[3] Brandrup J, Imergut EH. Polymer handbook. 3rd ed. New York; 1989.
[4] Cherdhirankorn T, Lerdwijitjarud W, Sirivat A, Larson LG. Rheol Acta 2004;43:246–56.
[5] De Bruijn RA. Ph.D. thesis. Eindhoven University of Technology; 1989.
[6] Elmendorp JJ, Maalcke RJ. Polym Eng Sci 1985;25:1041–7.
[7] Grace HP. Chem Eng Commun 1982;14:225–77.
[8] Guido S, Villone M. J Rheol 1998;42:395–415.
[9] Hobbie EK, Migler KB. Phys Rev Lett 1999;82:5393–6.
[10] Lerdwijitjarud W, Sirivat A, Larson RG. J Rheol 2004;48:843–62.
[11] Levitt L, Macosko CW, Pearson SD. Polym Eng Sci 1996;36:1647–55.
[12] Mighri F, Ajji A, Carreau PJ. J Rheol 1997;41:1183–201.

[13] Mighri F, Carreau PJ, Ajji A. J Rheol 1998;42:1477–90.
[14] Mighri F, Huneault MA. J Rheol 2001;45:783–97.
[15] Migler KB. J Rheol 2000;44:277–90.
[16] Rallison JM, Acrivos A. J Fluid Mech 1978;89:191–200.
[17] Taylor GI. Proc R Soc London Ser A 1932;138:41–8.
[18] Taylor GI. Proc R Soc London Ser A 1934;146:501–23.
[19] Varanasri PP, Ryan ME, Stroeve P. Ind Eng Chem Res 1994;33: 1858–66.